NANO LETTERS

pubs.acs.org/NanoLett

Large-Scale Arrays of Single-Layer Graphene Resonators

Arend M. van der Zande,*,† Robert A. Barton,‡ Jonathan S. Alden,‡ Carlos S. Ruiz-Vargas,‡ William S. Whitney,† Phi H. Q. Pham,¶ Jiwoong Park,§,∥ Jeevak M. Parpia,† Harold G. Craighead,‡ and Paul L. McEuen*,†,∥

†Laboratory of Atomic and Solid State Physics, ‡School of Applied and Engineering Physics, §Department of Chemistry, and ∥Kavli Institute at Cornell for Nanoscale Science, ⊥Cornell University, Ithaca, New York 14853, United States and ¶Department of Physics, University of Colorado, Boulder, Colorado 80309, United States

ABSTRACT We fabricated large arrays of suspended, single-layer graphene membrane resonators using chemical vapor deposition (CVD) growth followed by patterning and transfer. We measure the resonators using both optical and electrical actuation and detection techniques. We find that the resonators can be modeled as flat membranes under tension, and that clamping the membranes on all sides improves agreement with our model and reduces the variation in frequency between identical resonators. The resonance frequency is tunable with both electrostatic gate voltage and temperature, and quality factors improve dramatically with cooling, reaching values up to 9000 at 10 K. These measurements show that it is possible to produce large arrays of CVD-grown graphene resonators with reproducible properties and the same excellent electrical and mechanical properties previously reported for exfoliated graphene.

KEYWORDS Graphene, nanoelectro-mechanical systems, nanomechanics, NEMS, chemical vapor deposition, carbon

Graphene, a single layer of carbon atoms bonded in a hexagonal lattice, is the prototypical two-dimensional membrane. Its unparalleled strength, small mass per unit area, ultrahigh aspect ratio, and unusual electronic properties make it an ideal candidate for nanoelectro-mechanical systems (NEMS).[1−3] Previously, suspended graphene membranes could only be made in small batches using mechanical exfoliation,[1,2,4−7] growth on silicon carbide substrates,[8] or as graphene oxide.[3] These techniques are all extremely limiting, as they produce either very small numbers of devices, multilayer graphene on conducting substrates, or resistive functionalized graphene. The ideal solution should produce large numbers of single-layer graphene membranes while maintaining exfoliated graphene's excellent electronic and mechanical properties. In this letter, we demonstrate new methods to produce large arrays of suspended, single-layer graphene membrane resonators on arbitrary substrates using graphene grown by chemical vapor deposition (CVD). Having many membranes allows us to systematically study the mechanical resonance properties of single-layer graphene resonators as a function of size, clamping geometry, temperature, and electrostatic tuning. We find that the CVD graphene produces tensioned, electrically conducting, highly tunable resonators with properties equivalent to exfoliated graphene. In addition, we find that clamping the graphene membrane on all sides reduces the variation in resonance frequency and makes the behavior more predictable.

We started by using chemical vapor deposition to grow graphene on copper foil.[9] The graphene was verified to be predominantly single-layer (>90%) with low disorder by Raman microscopy and scanning electron microscopy (see Supporting Information).[10] We fabricated three different device geometries shown in Figures 1a, 3a, and 4a using variations on the graphene transfer technique developed by refs 9, 11, and 12. Type A membranes (Figure 1a−c) consist of graphene strips suspended over trenches and clamped at both ends (doubly clamped) by the van der Waals adhesion of the graphene to the substrate. We fabricated Type A membranes by patterning the graphene into strips on the copper foil with photolithography and oxygen plasma then transferring the patterned graphene onto trenches on a 285 nm silicon oxide substrate. Type B membranes (Figure 3a) are square graphene membranes clamped on all sides. We fabricated these membranes by transferring unpatterned graphene onto a suspended silicon nitride membrane with square holes. Type C membranes (Figure 4a) are electrically contacted membranes suspended between two gold electrodes fabricated by transferring unpatterned graphene to a 285 nm silicon oxide substrate, patterning the graphene into small bars, depositing gold electrodes on top, and suspending the graphene by wet etching the oxide out from underneath. Detailed fabrication procedures for all geometries are available in the Supporting Information.

With all approaches, we produce hundreds to hundreds of thousands of single-layer suspended graphene membranes in each fabrication run. For Type A and C devices,

* To whom correspondence should be addressed. E-mail: (A.M.v.d.Z.) amv28@cornell.edu; (P.L.M.) plm23@cornell.edu.

Received for review: 08/2/2010
Published on Web: 11/16/2010

DOI: 10.1021/nl102713c | *Nano Lett.* **2010,** *10,* 4869–4873

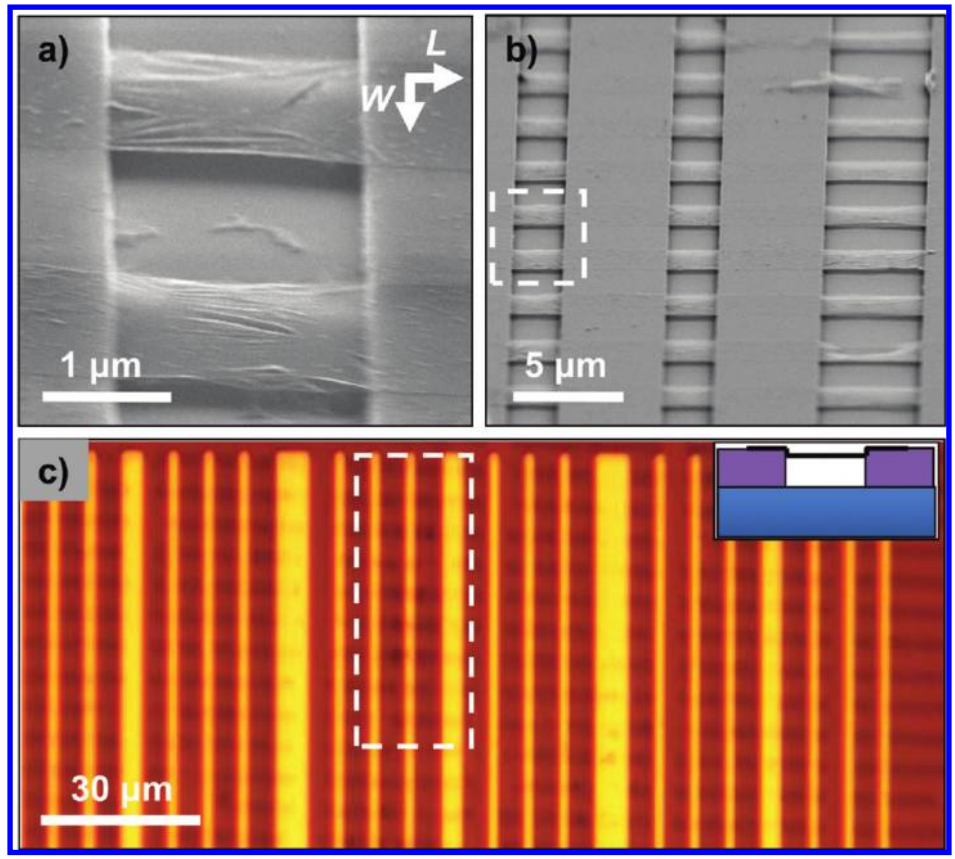

FIGURE 1. (a) Angled scanning electron microscopy (SEM) image of Type A suspended graphene membranes over trenches in silicon oxide. (b) Angled SEM of an array of graphene membranes. (c) Optical image of a large array of graphene membranes. Cross-section inset. Dashed rectangles indicate sizes of the regions in previous images, but the regions do not correspond exactly with each other.

we get yields of >80% for membranes with $L < 3\ \mu$m and $W < 5\ \mu$m. For type B devices, we get yields of >90% for membranes up to 5 μm on a side with lower yields for membranes up to 30 μm on a side.

The suspended graphene membranes show complicated conformational structure, including small-scale (~10 nm in amplitude) ripples such as those seen in Figure 1a, and larger-scale (~100 nm in amplitude) buckling of the membrane along the length and width. Ripples and buckling have also been observed in both exfoliated[6,13] and epitaxial[8] graphene membranes due to in-plane tension, shear, or compression. The amount of rippling and buckling in our devices varies between neighboring membranes produced on a single chip, indicating that the tension/shear/compression in the graphene membranes is variable. The degree to which this variability influences the resonator properties is addressed below. Finally, in larger membranes, occasional tears occur at mechanically weak grain boundaries between crystals in the CVD grown graphene.[14,15]

To actuate and detect the mechanical resonance of the graphene membranes, we first used a resonance-modulated optical reflectance measurement.[1,16] The membrane is actuated with a radio frequency (RF) modulated 405 nm CW laser, and the mechanical motion is detected using interferometry of the reflected light of a 633 nm helium−neon laser. All optical measurements were performed at room temperature in vacuum with $p < 5 \times 10^{-5}$ Torr.

Figure 2a is a plot of the fundamental mode for a Type A membrane of length $L = 2\ \mu$m and width $W = 3\ \mu$m. The resonance frequency is $f_1 = 9.77$ MHz and the quality factor is $Q = 52$. Figure 2b−d shows the frequency and quality factor of the fundamental mode for 38 identically patterned membranes measured along a single trench. Figure 2b,c are histograms of the resonance frequencies and quality factors. There is a clear peak in the histogram at $f_1 \sim 15$ MHz with a spread of 8 MHz. The quality factors range from 25−250 with a peak at 70. Figure 2d shows that higher frequency is correlated with higher quality factor. These resonators are nominally identical so the variation is due to either differences in adsorbed mass or the strain and conformational structure of the membranes.

Figure 2e shows f_1 versus L for Type A doubly clamped membranes with L between 1 and 6 μm and W between 2.5 and 5 μm, plotted on a log−log scale. The resonance frequencies decrease with length and show no discernible dependence on the width. For reference, the dashed line shows an L^{-1} dependence. The black dots represent graphene membranes without tears, while the squares represent partially torn membranes. Interestingly, the torn membranes show similar behavior to the untorn membranes.

DOI: 10.1021/nl102713c | *Nano Lett.* **2010,** *10,* 4869–4873

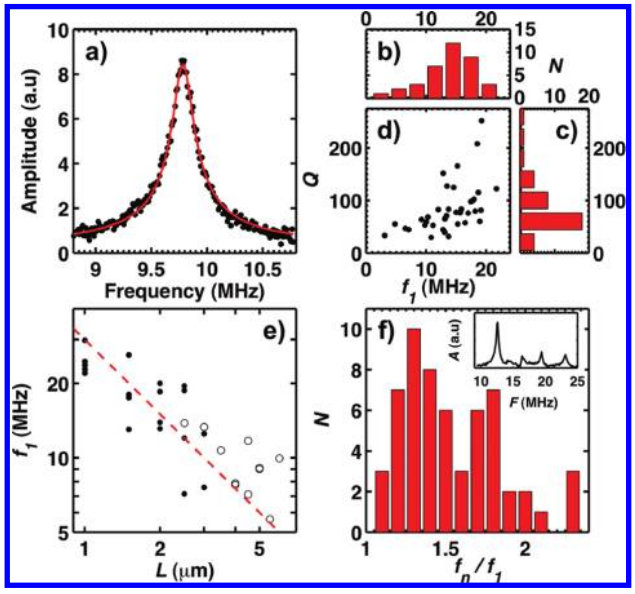

FIGURE 2. (a) Optical interferometry measurement of a fundamental mode for Type A graphene resonator like those shown in Figure 1a. $L = 2$ μm, $W = 3$ μm. Histogram of the frequency (b), and quality factor (c) of fundamental modes for 38 identical Type A resonators along a single trench $L = 2$ μm, $W = 3$ μm. (d) Quality factor versus resonance frequency for the same devices as panels b,c. (e) Fundamental mode frequency versus length for membranes with widths W between 2.5 and 5 μm. Solid dots are continuous, damage-free membranes, open circles are membranes with partial tears in them. Dashed line shows data scales as $1/L$. (f) Histogram of all measured higher modes divided by the fundamental mode for same devices as Figure 2b−d. Typical resonance spectrum inset.

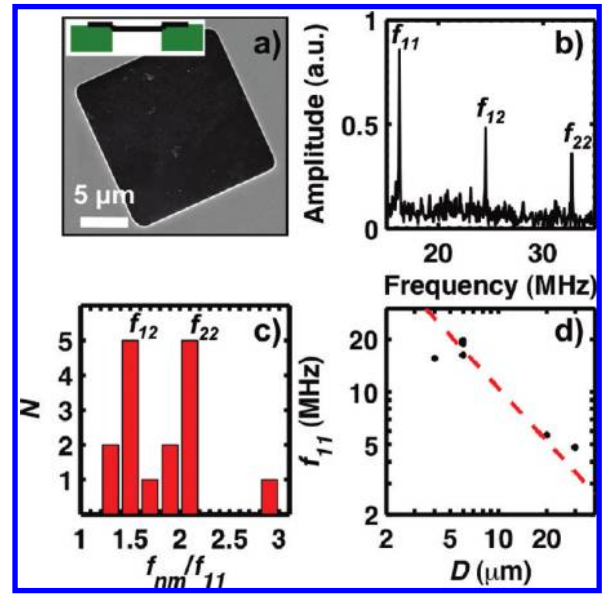

FIGURE 3. (a) SEM of a Type B, side-length $D = 30$ μm square graphene membrane on a suspended silicon nitride membrane. Without a substrate behind the graphene to adjust the contrast, the absorbed mass contamination is clearly visible on the graphene. (b) Typical spectrum for a Type B, $D = 6$ μm square membrane. (c) Histogram of all measured higher modes divided by the fundamental mode for square membranes. Higher modes occur at predictable intervals for square membranes. (d) Fundamental mode frequency versus side length D for square membranes. Dashed line shows data scales as $1/D$.

The simplest model of a doubly clamped graphene membrane resonator is as a sheet under tension[1,2,4,5,7]

$$f_n = \frac{n}{2L}\sqrt{\frac{Yt}{\rho_0}\frac{s}{\alpha}} \tag{1}$$

where Yt = 340 N/m and $\rho_0 = 7.4 \times 10^{-7}$ kg/m^2 are the in-plane stiffness and density of single-layer graphene, $n = 1$, 2, 3... is the mode number, s is the in-plane strain, and $\alpha = \rho_{total}/\rho_0$ is the adsorbed mass coefficient. Previous results[4,5,7] have shown the ratio of the contamination mass to the membrane mass can be large, typically varying between 1 and 10. This model predicts a L^{-1} scaling of the resonance frequencies with length, consistent with the data. From a best fit to the data in Figure 2e, we extract the average strain per absorbed mass ratio on the resonators of $s/\alpha \sim 10^{-5}$. This value is comparable to previously measured strains on exfoliated graphene membranes.[4,5,7] The strain likely results from the self-tensioning of the graphene as the van der Waals attraction adheres the membrane to the walls of the trench, as shown schematically in the Figure 1 inset.[7,17,18]

The tensioned membrane model predicts a second harmonic at twice the frequency of the first. Figure 2f shows all measured higher resonant modes of the identical devices, normalized by the fundamental mode frequency with one example spectrum in the inset. Instead of a peak at $2f_1$, there is a broad distribution in frequencies with peaks around $f_n \sim 1.3 f_1$ and $1.6 f_1$. These peaks correspond with the second and third measured modes. These most likely correspond to transverse modes or edge modes in the resonator due to nonuniform strain in the resonator. Previous experiments[6] have shown that local modes can exist at the edges exist in exfoliated graphene resonators and the frequencies of these modes are difficult to estimate without a detailed knowledge of the structure in the transverse direction.

To test the hypothesis that the transverse properties are important, we fabricated and measured the resonance in the Type B membranes shown in Figure 3a, where the membrane is clamped on all sides and the transverse modes are identical to the longitudinal ones. Figure 3b,c shows that we observe higher resonant modes at frequencies approximately 1.5 and 2 times the fundamental. This is in good agreement with the expected values of $f_{21} = 1.58\, f_{11}$, and $f_{22} = 2f_{11}$ predicted for a square membrane of uniform tension clamped on all sides

$$f_{nm} = \frac{\sqrt{n^2 + m^2}}{2D}\sqrt{\frac{Yt}{\rho_0}\frac{S}{\alpha}} \tag{2}$$

With the fully clamped membranes, the reproducibility is also improved with frequencies of 16.5, 18.8, 19.4, and

DOI: 10.1021/nl102713c | Nano Lett. 2010, 10, 4869–4873

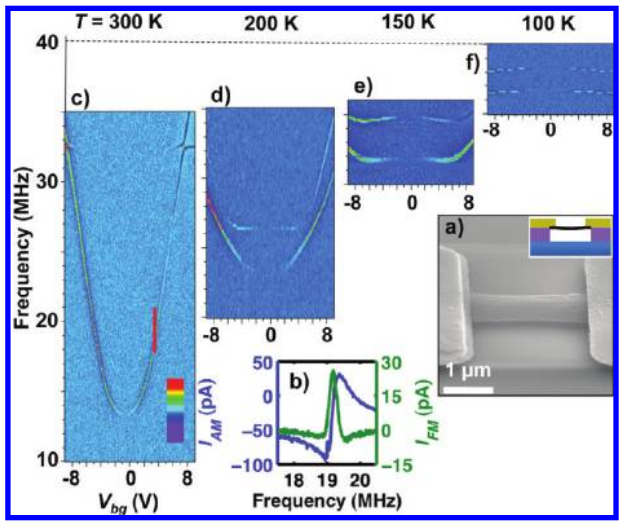

FIGURE 4. (a) Angled SEM image of electrically isolated suspended graphene clamped to gold electrodes with a degenerately doped silicon backgate. Schematic of cross-section inset. (b) Electrical mixing measurement of mechanical resonance of membrane shown in panel a versus frequency, measured using AM (blue) and FM (green) mixing techniques for $V_{bg} = 3$ V, $V_{rf} = 7$ mV. (c) FM mixing signal (colorscale = −100 to 100 pA) versus gate voltage and drive frequency at room temperature. The resonance frequency is tuned by the electrostatic gate voltage. Red line indicates cut taken to get FM data shown in panel b. (d−f) The evolution of the tuning for the same resonator at $T = 200$, 150, and 100 K, respectively.

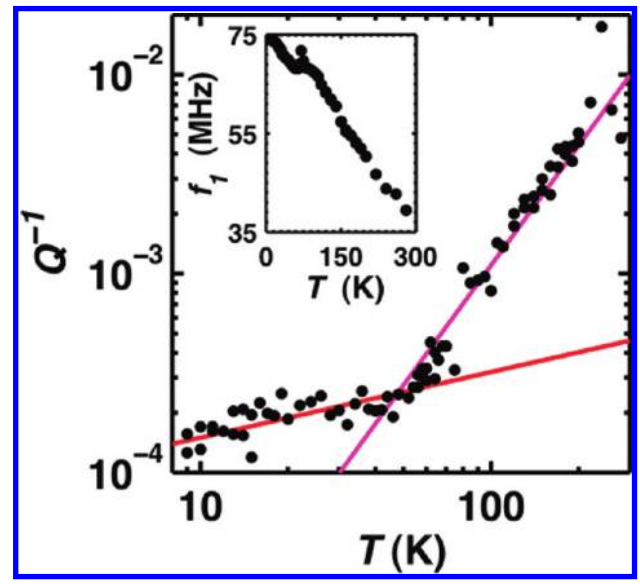

FIGURE 5. Inverse quality factor versus temperature at a $V_{bg} = 3$ V; red and magenta lines show data scales as $T^{1/3}$ and $T^{2.3}$, respectively. Frequency versus temperature inset.

19.8 MHz measured for four nominally identical devices, a spread of less than 15%. The frequency also scales as approximately the inverse of the membrane dimension, as shown in Figure 3d. The quality factors are also higher, $Q >$ 200; noise prevents a more accurate determination. Full clamping clearly improves the device reproducibility and quality factors over those observed in doubly clamped membranes, likely by eliminating soft degrees of freedom associated with the free edges.

Some of the most exciting properties of exfoliated graphene resonators are their ability to be actuated and detected electrically,[4] their large voltage-tunable frequency range and their high quality factor at low temperature ($Q \sim$ 10 000 for exfoliated graphene at 4 K[4]). We explored these aspects of CVD graphene resonators by fabricating the Type C, electrically contacted resonators shown in Figure 4a. Transport measurements (see Supporting Information) show these devices have mobilities of 1000−4000 $cm^2/V \cdot s$, similar to previous results on CVD graphene.[9,19] Using the electromechanical mixing measurement reported by Chen et al.,[4] we actuated the resonators electrostatically and measured the motion using amplitude modulation (AM)[4,20,21] or frequency modulation (FM)[22,23] mixing (details in the Supporting Information). Figure 4b shows the electrical mixing response versus drive frequency for AM (blue) and FM (green) mixing techniques with back gate voltage $V_{bg} =$ 3 V, and drive $V_{RF} = 7$ mV. Both techniques yield a resonator frequency $f_1 = 19.2$ MHz and quality factor of $Q = 44$ at this gate voltage.

Figure 4c shows the FM mixing current as a function of the drive frequency and electrostatic gate voltage at room temperature. The resonance frequency increases by more than a factor of 2 for large V_{bg} and is symmetric around a minimum close to $V_{bg} = 0$, very similar to the behavior previously reported for exfoliated graphene.[4,5]

Figure 4(d−f) shows the tuning of the same resonance at $T = 200$, 150, and 100 K. As the temperature is decreased the frequency of the resonator at $V_{bg} = 0$ rises, while the dependence of the resonance frequency on V_{bg} becomes weaker, and even reverses sign at 100 K. The change of frequency tunability with temperature is due to changes in the tension of the graphene as it is cooled and is similar to that seen in exfoliated graphene resonators.[4,5] Figure 5 shows the inverse quality factor of a resonator versus temperature for a fixed $V_{bg} = 3$ V. The inset shows the frequency versus temperature over the same temperature range. As the temperature is decreased, the quality factor rises dramatically from 150 at room temperature to 9000 at 9 K. This is comparable to the highest quality factors reported for graphene resonators at that temperature.[4]

From Figure 5, the inverse quality factor scales approximately as T^{α} where $\alpha = 0.35 \pm 0.05$ from 9 up to 40 K, and as T^{β} where $\beta = 2.3 \pm 0.1$ from 40 K to room temperature. The temperature scaling is similar to what is found for exfoliated graphene resonators.[4] Similar temperature dependence is also seen in carbon nanotube resonators.[21,24] While there are many theories examining dissipation in these systems[25−28] the observed behavior is still not understood.

The techniques described here provide a step toward practical graphene-based devices. This work shows that it is possible to fabricate large arrays of low mass, high aspect ratio, CVD-grown single-layer graphene membranes while maintaining the

DOI: 10.1021/nl102713c | Nano Lett. 2010, 10, 4869–4873

remarkable electronic and mechanical properties previously observed for exfoliated graphene. This is an important conclusion, demonstrating that the benefit of wafer-scale processing allowed by CVD graphene comes at little or no cost in mechanical resonator performance. We further show that clamping the membrane on all sides improves resonator performance and reproducibility. The wafer-scale production of low-mass, high-frequency, and highly tunable nanomechanical membrane resonators opens the way for applications in areas from sensing to signal processing.

Acknowledgment. This work was supported by the NSF through the Cornell Center for Materials Research (CCMR), the MARCO Focused Research Center on Materials, Structures, and Devices, and the AFOSR MURI and PECASE grants. Sample fabrication was performed at the Cornell node of the National Nanofabrication Infrastructure Network, funded by the NSF. We thank Kit Umbach and Pinshane Huang for help in characterizing the CVD graphene and Alan Zehnder for useful discussions.

Supporting Information Available. Detailed graphene growth, transfer, and nanofabrication procedures, as well as a brief discussions of sample quality, tearing in graphene membranes, electrical transport measurement, and a derivation of electrical mixing measurements. This material is available free of charge via the Internet at http://pubs.acs.org.

REFERENCES AND NOTES

(1) Bunch, J. S.; Van Der Zande, A. M.; Verbridge, S. S.; Frank, I. W.; Tanenbaum, D. M.; Parpia, J. M.; Craighead, H. G.; Mceuen, P. L. *Science* **2007**, *315* (5811), 490–493.
(2) Lee, C.; Wei, X. D.; Kysar, J. W.; Hone, J. *Science* **2008**, *321* (5887), 385–388.
(3) Robinson, J. T.; Zalalutdinov, M.; Baldwin, J. W.; Snow, E. S.; Wei, Z.; Sheehan, P.; Houston, B. H. *Nano Lett.* **2008**, *8* (10), 3441–3445.
(4) Chen, C.; Rosenblatt, S.; Bolotin, K. I.; Kalb, W.; Kim, P.; Kymissis, I.; Stormer, H. L.; Heinz, T. F.; Hone, J. *Nat. Nanotechnol.* **2009**, 1–7.
(5) Singh, V.; Sengupta, S.; Solanki, H. S.; Dhall, R.; Allain, A.; Dhara, S.; Pant, P.; Deshmukh, M. M. *Nanotechnology* **2010**, *21* (16), 165204.
(6) Garcia-Sanchez, D.; van der Zande, A. M.; Paulo, A. S.; Lassagne, B.; McEuen, P. L.; Bachtold, A. *Nano Lett.* **2008**, *8* (5), 1399–1403.
(7) Bunch, J. S.; Verbridge, S. S.; Alden, J. S.; van der Zande, A. M.; Parpia, J. M.; Craighead, H. G.; McEuen, P. L. *Nano Lett.* **2008**, *8* (8), 2458–2462.
(8) Shivaraman, S.; Barton, R. A.; Yu, X.; Alden, J.; Herman, L.; Chandrashekhar, M.; Park, J.; Mceuen, P. L.; Parpia, J. M.; Craighead, H. G.; Spencer, M. G. *Nano Lett.* **2009**, *9* (9), 3100–3105.
(9) Li, X.; Cai, W.; An, J.; Kim, S.; Nah, J.; Yang, D.; Piner, R.; Velamakanni, A.; Jung, I.; Tutuc, E.; Banerjee, S. K.; Colombo, L.; Ruoff, R. S. *Science* **2009**, *324* (5932), 1312–1314.
(10) Ferrari, A.; Meyer, J.; Scardaci, V.; Casiraghi, C.; Lazzeri, M.; Mauri, F.; Piscanec, S.; Jiang, D.; Novoselov, K.; Roth, S.; Geim, A. *Phys. Rev. Lett.* **2006**, *97* (18), 187401.
(11) Kim, K. S.; Zhao, Y.; Jang, H.; Lee, S. Y.; Kim, J. M.; Kim, K. S.; Ahn, J.-H.; Kim, P.; Choi, J.-Y.; Hong, B. H. *Nature* **2009**, *457* (7230), 706–710.
(12) Reina, A.; Jia, X.; Ho, J.; Nezich, D.; Son, H.; Bulovic, V.; Dresselhaus, M. S.; Kong, J. *Nano Lett.* **2009**, *9* (8), 3087–3087.
(13) Bao, W.; Miao, F.; Chen, Z.; Zhang, H.; Jang, W.; Dames, C.; Lau, C. N. *Nat. Nanotechnol.* **2009**, *4* (9), 562–566.
(14) Grantab, R.; Shenoy, V.; Ruoff, R. S. arXiv 2010, cond-mat.mtrl-sci (1007.4985v1). Accessed July 28, 2010.
(15) Huang, P. Y.; Ruiz-Vargas, C. S.; Zande, A. M. v. d.; Whitney, W. S.; Garg, S.; Alden, J. S.; Hustedt, C. J.; Zhu, Y.; Park, J.; McEuen, P. L.; Muller, D. A. arXiv 2010, cond-mat.mtrl-sci. Accessed July 28, 2010.
(16) Carr, D.; Sekaric, L.; Craighead, H. *J. Vac. Sci. Technol. B* **1998**, *16* (6), 3821−3824.
(17) Hertel, T.; Walkup, R. E.; Avouris, P. *Phys. Rev. B* **1998**, *58* (20), 13870.
(18) Ruoff, R. S.; Tersoff, J.; Lorents, D. C.; Subramoney, S.; Chan, B. *Nature* **1993**, *364* (6437), 514–516.
(19) Levendorf, M. P.; Ruiz-Vargas, C. S.; Garg, S.; Park, J. *Nano Lett.* **2009**, *9* (12), 4479–4483.
(20) Sazonova, V.; Yaish, Y.; Ustunel, H.; Roundy, D.; Arias, T. A.; McEuen, P. L. *Nature* **2004**, *431* (7006), 284–287.
(21) Sazonova, V. Ph.D. Thesis, Cornell University, Ithaca, NY, 2006.
(22) Jensen, K.; Weldon, J.; Garcia, H.; Zettl, A. *Nano Lett.* **2007**, *7* (11), 3508–3511.
(23) Gouttenoire, V.; Barois, T.; Perisanu, S.; Leclercq, J.-L.; Purcell, S. T.; Vincent, P.; Ayari, A. *Small* *6* (9), 1060–1065.
(24) Huttel, A. K.; Steele, G. A.; Witkamp, B.; Poot, M.; Kouwenhoven, L. P.; van der Zant, H. S. J. *Nano Lett* **2009**, *9* (7), 2547–2552.
(25) Seoanez, C.; Guinea, F.; Castro, A. H. *Phys. Rev. B* **2007**, *76* (12), 125427.
(26) Kim, S. Y.; Park, H. S. *Appl. Phys. Lett.* **2009**, *94* (10), 101918.
(27) Jiang, H.; Yu, M.-F.; Liu, B.; Huang, Y. *Phys. Rev. Lett.* **2004**, *93* (18), 185501.
(28) Lischner, J.; Arias, T. A. *Phys. Rev. B* **2010**, *81* (23), 233409.

DOI: 10.1021/nl102713c | *Nano Lett.* **2010,** *10,* 4869–-4873